

Supporting Information

Boosting Performance and Stability of Inverted Perovskite Solar Cells Enabled by Using a Carbolong Derivative to Modulate Cathode Interface

Jinhua Li,^{a, f, ‡} Jiantao Wang,^{b, ‡} Yecheng Zhou,^{c, ‡} Chengzhuo Yu,^b Heng Liu,^b Xingnan Qi,^b Ruxue Li,^d Yuhui Hua,^{a, f} Yinye Yu,^c Rui Chen,^d Dafa Chen,^a Lingling Mao,^a Haiping Xia^{*a, f} and Hsing-Lin Wang^{*b, c}

^a*Department of Chemistry, Shenzhen Grubbs Institute, Southern University of Science and Technology, Xueyuan Avenue 1088, Shenzhen 518055, China. Email: xiahp@sustech.edu.cn.*

^b*Department of Materials Science and Engineering, Southern University of Science and Technology, Xueyuan Avenue 1088, Shenzhen 518055, China. Email: wangxl3@sustech.edu.cn.*

^c*School of Materials Science and Engineering, Sun Yat-sen University, Zhongshan West Road 135, Guangzhou 510275, China.*

^d*Department of Electrical and Electronic Engineering, Southern University of Science and Technology, Xueyuan Avenue 1088, Shenzhen 518055, China.*

^e*Guangdong Provincial Key Laboratory of Energy Materials for Electric Power, Southern University of Science and Technology, Xueyuan Avenue 1088, Shenzhen 518055, China.*

^f*Department of Chemistry, College of Chemistry and Chemical Engineering, Xiamen University, Xiamen 361005, China.*

[‡] *These authors contributed equally to this work.*

1. General Information

Formamidinium Iodide (FAI, >99.95%), Methylammonium Bromide (MABr, >99.95%), Lead (II) Dibromide (PbBr_2 , 99.99%), and Poly[bis(4-phenyl)(2,4,6-trimethylphenyl)amine] (PTAA, $M_n=6,000-15,000$) were purchased from Xi'an Polymer Light Technology Corp. (China). Indium Tin Oxide (ITO) glasses and Lead (II) Diiodide (PbI_2 , 99.999%) were purchased from Advanced Election Technology Co., Ltd. (China). Chlorobenzene (CB), Dimethyl Sulfoxide (DMSO), N, N-dimethylformamide (DMF), and Anhydrous Ethanol were purchased from *J&K*. Phenyl- C_{61} -butyric acid methyl ester (PC_{61}BM , 99.5%) were purchased from Shanghai Da Ran Chemicals (China). Silver (Ag, 99.99%) and Gold (Au, 99.99%) were obtained from commercial sources. Diethyl ether was distilled from sodium/benzophenone and dichloromethane from calcium hydride under N_2 prior to use. The reagents were used as received from commercial sources without further purification. NMR spectroscopic experiments were performed on a Bruker AVIII-400 (^1H , 400.1, ^{13}C , 100.6, ^{31}P , 162.0 MHz) spectrometer at room temperature. The ^1H and ^{13}C NMR chemical shifts (δ) are reported relative to tetramethylsilane, and the ^{31}P NMR chemical shifts are relative to 85% H_3PO_4 . The absolute values of the coupling constants are given in hertz (Hz). Multiplicities are abbreviated as singlet (s), doublet (d), triplet (t), multiplet (m), and broad (br). HRMS experiments were performed on a Bruker En Apex Ultra 7.0T FT-MS.

2. Spectroscopic and HRMS Data of compound 1:

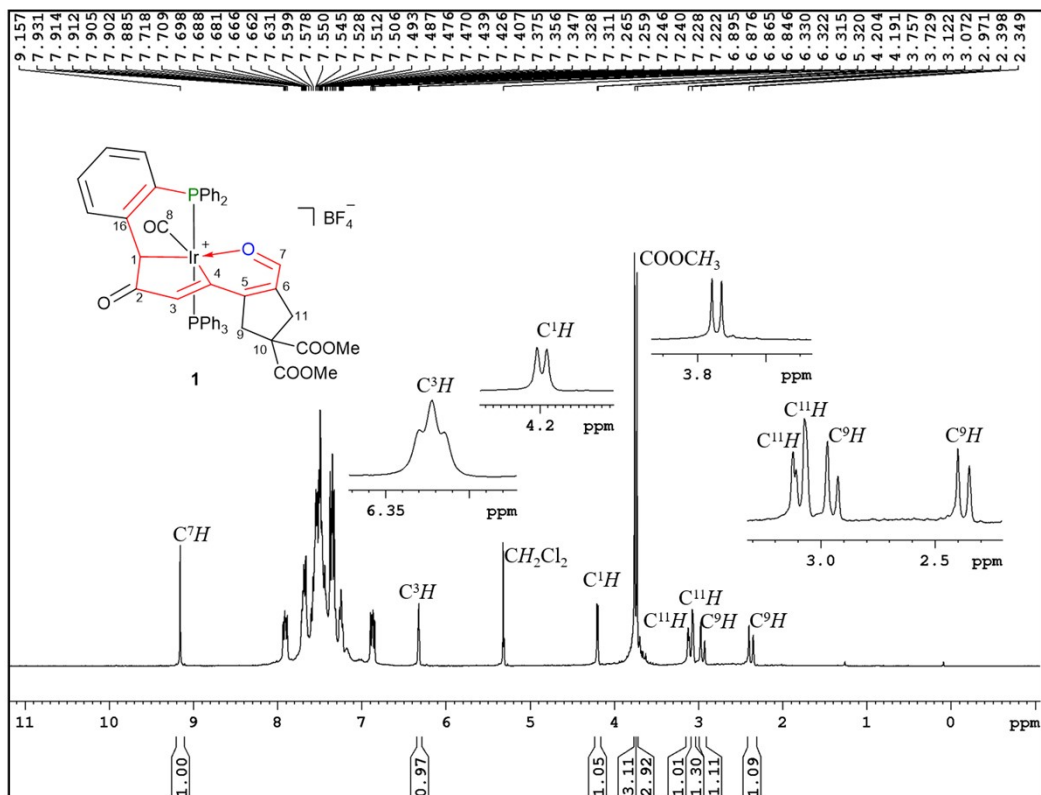


Figure S1. The ^1H NMR (400.0 MHz, CD_2Cl_2) spectrum of compound **1**.

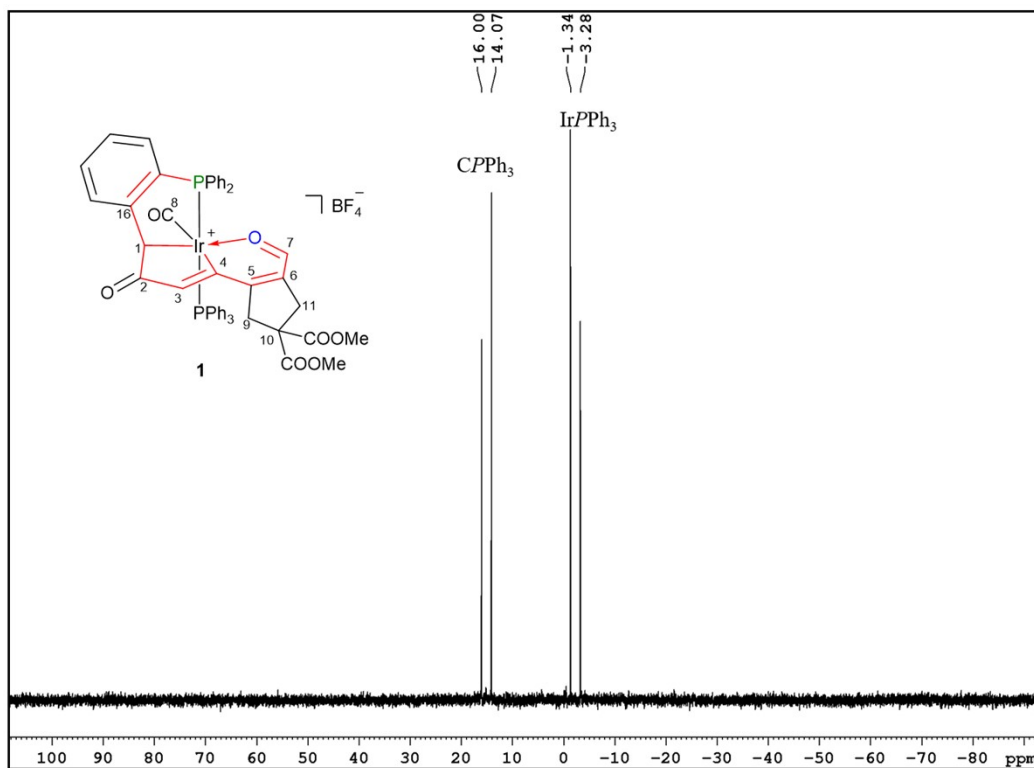


Figure S2. The $^{31}\text{P}\{^1\text{H}\}$ NMR (161.9 MHz, CD_2Cl_2) spectrum of compound **1**.

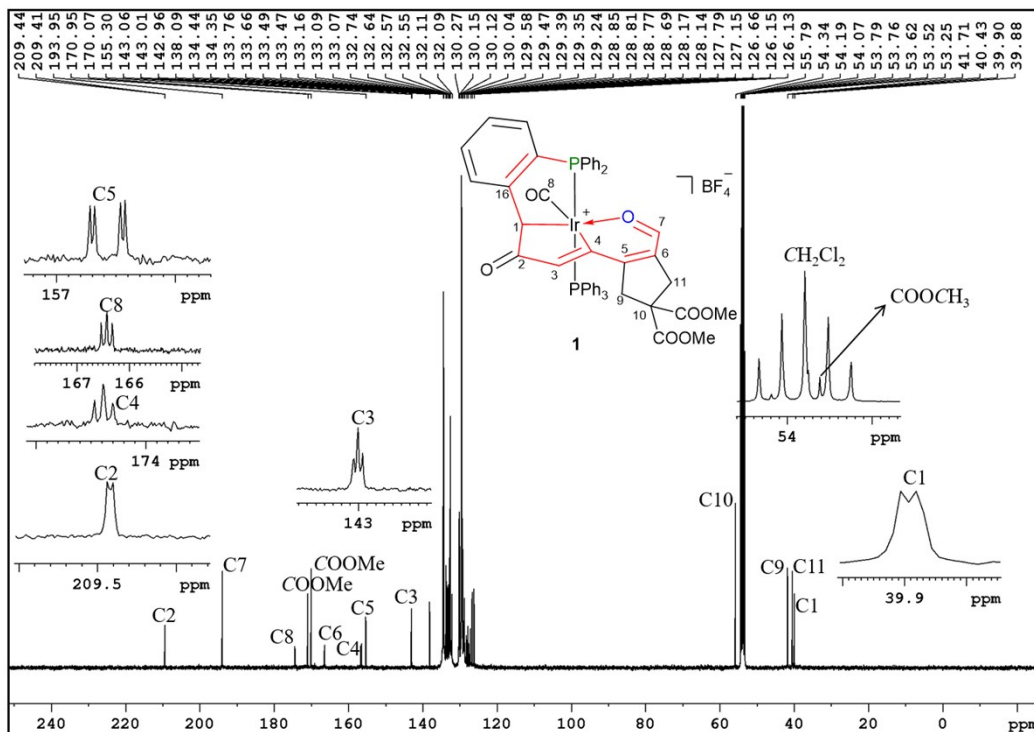


Figure S3. The $^{13}\text{C}\{^1\text{H}\}$ NMR (100.6 MHz, CD_2Cl_2) spectrum of compound **1**.

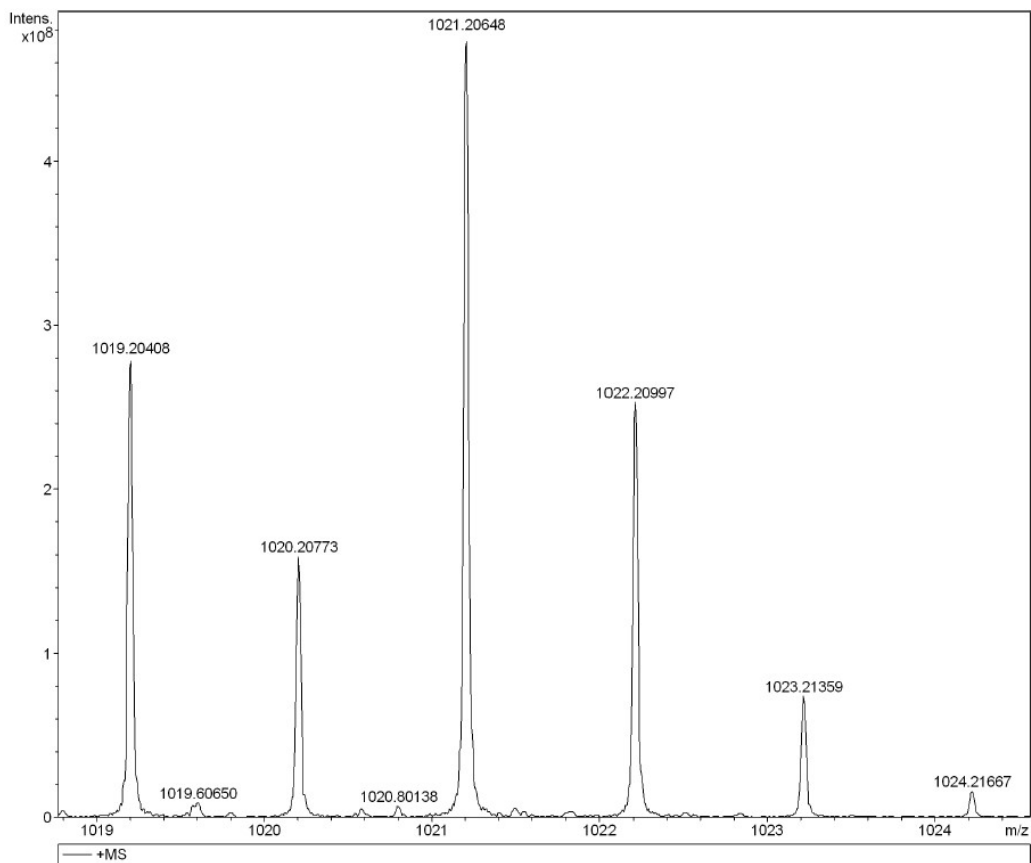


Figure S4. Positive ion ESI-MS spectrum of $[1\text{-BF}_4]^+ [\text{C}_{51}\text{H}_{42}\text{IrO}_7\text{P}_2]^+$ measured in methanol.

3. Characterizations of perovskite films

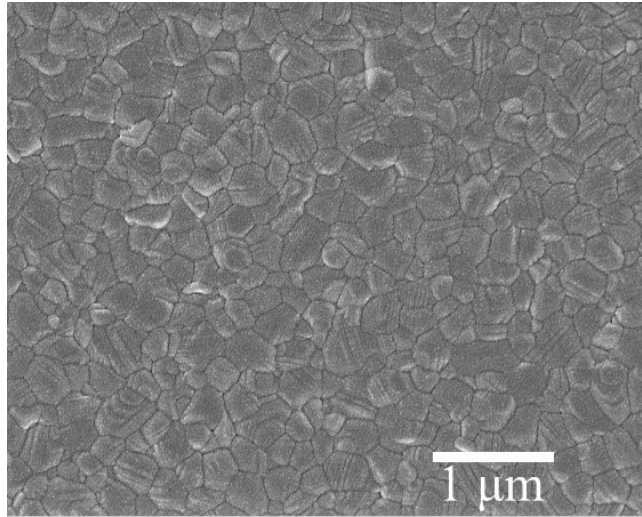


Figure S5. SEM surface morphology of perovskite film. Perovskite film was deposited on ITO substrate. The film is dense and pin-hole free, which is helpful for interface contact with PC₆₁BM, and avoid the leakage current.

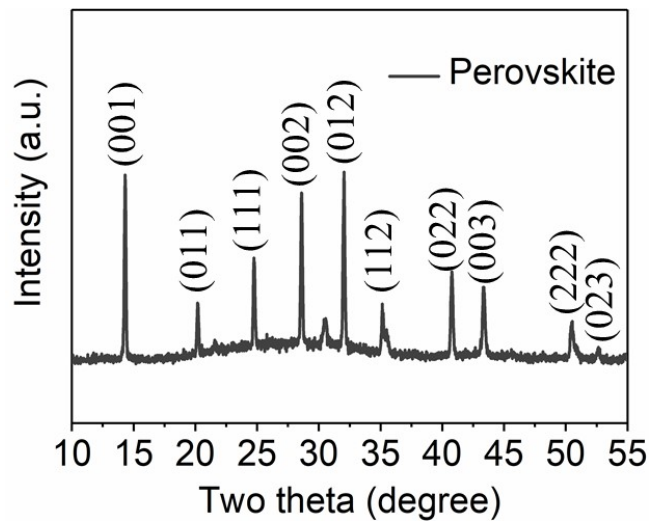


Figure S6. XRD curves of perovskite film. Perovskite film was deposited on ITO substrate. The XRD peaks at 14.3°, 20.2°, 24.7°, 28.6°, 30.1°, 35.1°, 40.8°, 43.4°, 50.5° and 52.7° correspond to the characteristic peaks (001), (011), (111), (002), (012), (112), (022), (003), (222), and (023) of FAPbI₃ based compositions. The peak located at 30.5° is from the ITO substrate.

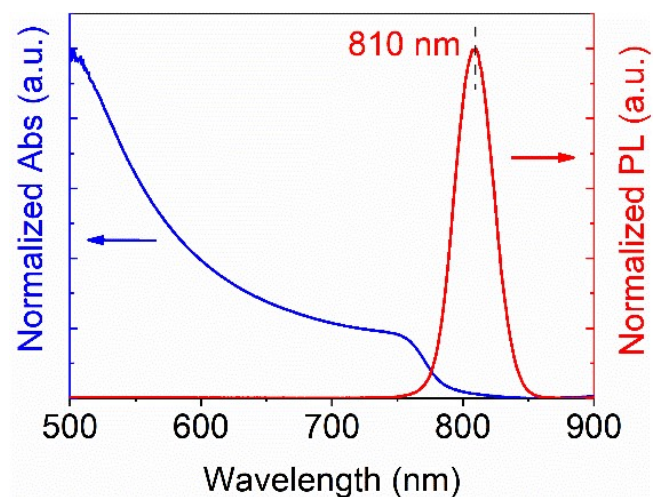


Figure S7. UV-Vis absorption and photoluminescence (PL) curves of perovskite film. Perovskite film was deposited on quartz substrate. According to the absorption curve, the bandgap of perovskite layer is 1.56 eV. The PL peak is 810 nm, excited with a 540 nm incident light.

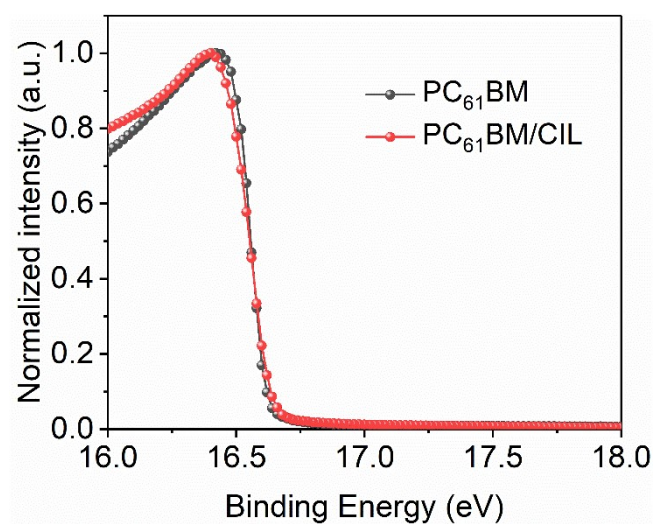


Figure S8. UPS results of PC₆₁BM with and without CIL.

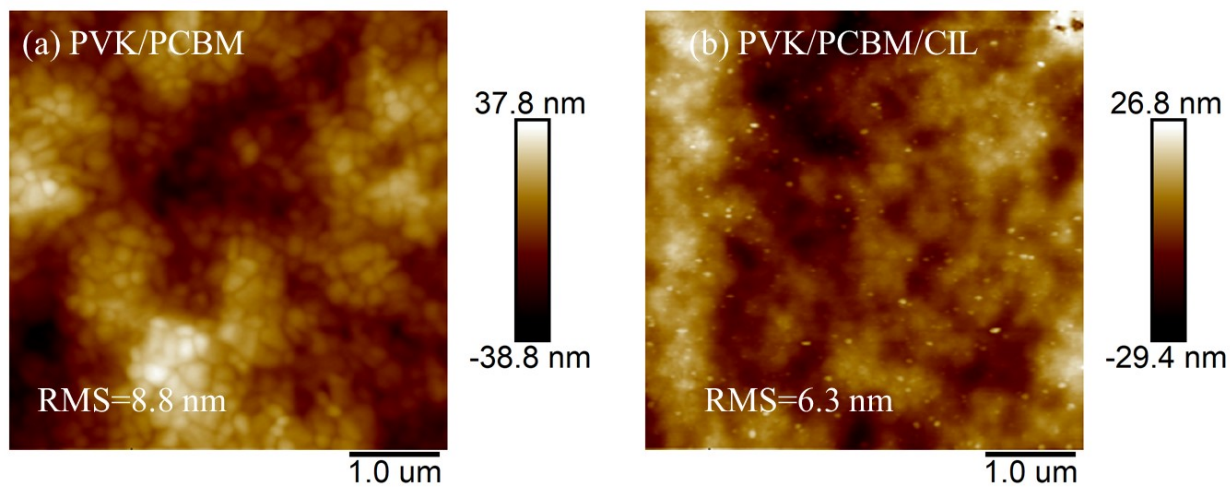


Figure S9. AFM mapping of (a) PVK/PCBM and (b) PVK/PCBM/CIL. Their root-mean-square (RMS) values are 8.8 nm and 6.3 nm, respectively. The introduction of CIL reduces the roughness of PCBM surface.

4. Molecular adsorption model construction

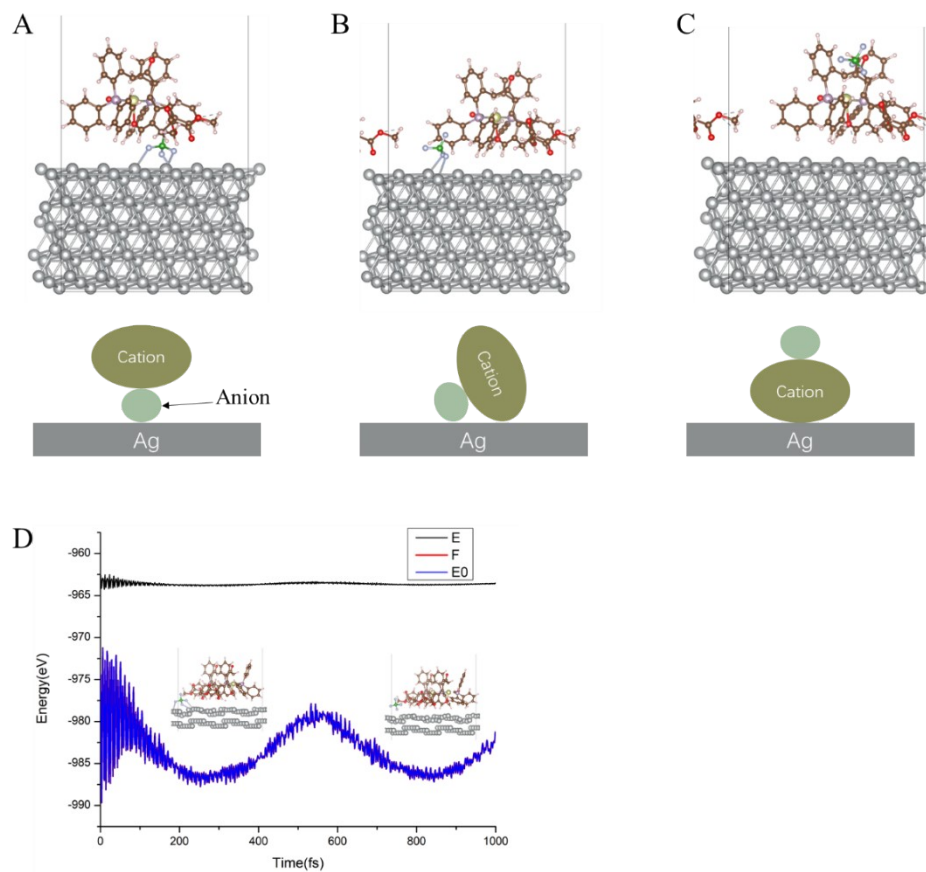


Figure S10. Adsorption configurations of carbolong derivative **1** on Ag surface and molecular dynamics simulation. The total energies for configurations (A) bottom anion-top cation, (B) anion-cation laydown and (C) bottom cation-top anion are -1509.648 eV, -1510.555 eV and -1509.364 eV, respectively. Configuration (B) is more favorable due to the lowest energy and was further used to perform the (D) molecular dynamics simulation to obtain the final molecular configuration.

5. Au WF reduction characterizations

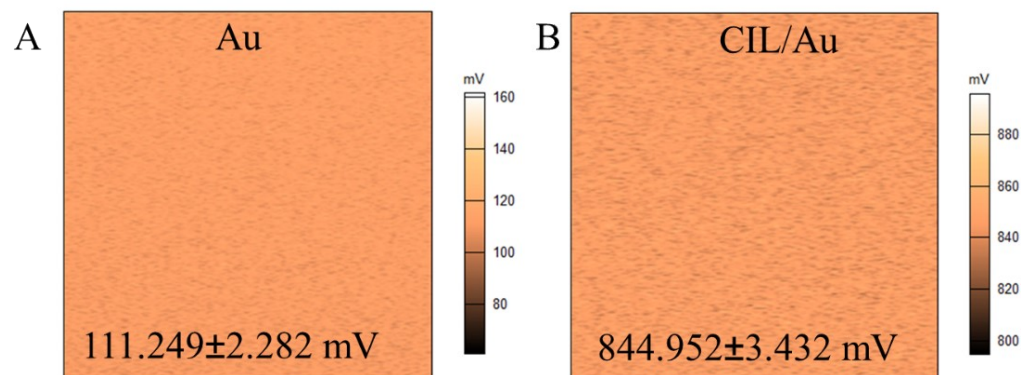


Figure S11. SKPM mappings of Au (A) before and (B) after the deposition of CIL. The surface potential of bare Au is 111.249 ± 2.282 mV while the CIL/Au is 844.952 ± 3.432 mV. A higher surface potential corresponds to a lower surface WF. Therefore, the Au WF is reduced after the employment of CIL.

6. Water contact angel measurements

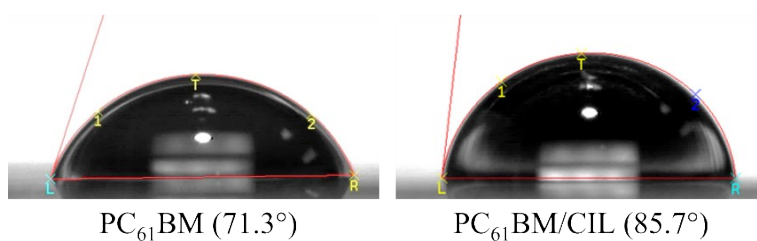


Figure S12. Water contact angle of PC₆₁BM and PC₆₁BM/CIL, respectively.

7. X-ray Crystallographic Analysis

The crystal of compound **1** suitable for X-ray diffraction was grown from the CH₂Cl₂ solution layered with ethyl ether. Single-crystal X-ray diffraction data were collected on XtaLAB Synergy, Dualflex, HyPix Area Detector with mirror-monochromated Cu K α radiation ($\lambda = 1.54184$ Å). All the Data were corrected for absorption effects using the multi-scan technique. Using Olex2^[S1], the

structure of compound **1** was solved with the ShelXT^[S2] structure solution program using Intrinsic Phasing; the structure was refined with the ShelXL^[S3] refinement package using least-squares minimization. All the non-hydrogen atoms were refined anisotropically unless otherwise stated. The hydrogen atoms were placed at their idealized positions and refined using a riding model unless otherwise stated. The solvents CH₂Cl₂, H₂O and phenyl groups on PPh₃ were disordered and refined by using restraints. Further details on the crystal data, data collection, and refinements are provided in Tables S5.

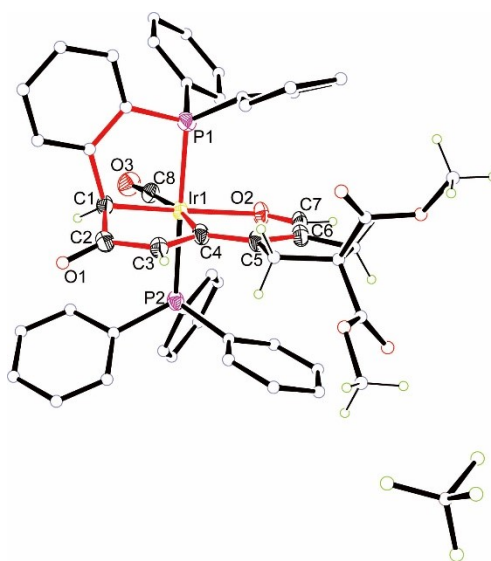


Figure S13. X-ray molecular structures of **1** (thermal ellipsoids set at 50% probability). The solvents and hydrogen atoms of phenyl moieties have been omitted for clarity.

8. DFT calculation

The molecular optimization was calculated at the **M06L/6-31G*** level with SDD for iridium atoms.^[S4] The energies of their molecular orbitals were further calculated at the B3PW91/def2-TZVP level.^[S5] The above calculations were performed in Gaussian 09D.01 packages.^[S6] Molecule adsorption calculations were performed by the Vienna Ab initio Simulation Package (VASP, Version 5.4.4), which is implemented with plane waves and the Projector-Augmented Wave

method. Both Perdew–Burke– Ernzerhof (PBE) functionals.^[S7] The energy cutoff was 550 eV and a Γ -centered $3\times 3\times 3$ k-mesh were used. Five-layer Ag slab model was built, and the surface area of this substrate was $22.1 \times 17.5 \text{ \AA}^2$. The adsorption concentration was $3.87/\text{nm}^2$. The configuration with the lowest energy was chosen for dipole and work function analysis.

Table S1. Photovoltaic parameters (best device and average values) of inverted PSCs based on Ag cathode.

CIL	Scan direction	V_{oc} [V]	J_{sc} [mA cm^{-2}]	FF [%]	PCE [%]
Without	Forward	1.08	22.74	66.88	16.44
	Reverse	1.08	22.79	70.38	17.39
	Average	1.07 ± 0.01	22.52 ± 0.77	69.94 ± 3.1	15.21 ± 1.42
With	Forward	1.07	24.03	79.75	20.55
	Reverse	1.08	23.88	83.14	21.46
	Average	1.07 ± 0.01	23.43 ± 0.64	81.23 ± 2.55	19.61 ± 0.9
BCP	Forward	1.05	21.36	79.93	17.92
	Reverse	1.07	21.57	82.40	19.02
	Average	1.06 ± 0.01	21.38 ± 0.72	80.16 ± 2.93	18.29 ± 1.29

Table S2. Device performance of typical PSCs under reverse scan based on different CIL thicknesses.

Thickness [nm]	V_{oc} [V]	J_{sc} [mA cm^{-2}]	FF [%]	PCE [%]
6	1.06	23.69	78.54	19.72
8	1.08	23.88	83.14	21.46
10	1.08	23.21	80.99	20.3
12	1.05	22.97	77.43	18.67

Table S3. Comparison of device performance of this work with other reported literatures.

Year	Journal	Perovskite composition	CIL/Cathode	PCE
2022	This work	CsFAMA	Control, W/o CIL/Ag	17.39%
			Control, BCP/Ag	19.02%
			Carbolong derivative/Ag	21.46%
			Control, W/o CIL/Au	14.11%
			Carbolong derivative/Au	20.82%
2022	J. Mater. Chem. A (DOI: 10.1039/d1ta10185d)	MAPbI ₃	Control, W/o CIL/Cu	15.9%
			Control, BCP/Cu	18.33%
			CzNBr/Cu	20.28%
2021	J. Am. Chem. Soc. (DOI: 10.1021/jacs.1c02118)	CsFAMA	Control, W/o CIL/Ag	17.13%
			Organometallic material/Ag	21.29%
			Control, W/o CIL/Au	14.24%
2021	Nano Energy (DOI: 10.1016/j.nanoen.2021.106374)	MAPbI ₃	Control, W/o CIL/Ag	16.4%
			PPDIBPP/Ag	20.2%
2020	Sci. Adv. (DOI: 10.1126/sciadv.abd1580)	(FAPbI ₃) _{0.95} (MAPbBr ₃) _{0.05}	Control, TPBi/Cu	20.15%
			TPBi/BTA/Cu	19.56%

Table S4. Fitting parameters of TRPL curves of inverted PSCs based on Ag cathode.

CIL	A1 [%]	τ_1 [ns]	A2 [%]	τ_2 [ns]	τ_{av} [ns]
Without	37.96	16.667	62.04	49.784	37.212
With	23.24	6.280	76.76	27.191	22.332

Table S5. Photovoltaic parameters (best device and average values) of inverted PSCs based on Au cathode.

CIL	Scan direction	V_{oc} [V]	J_{sc} [mA cm ⁻²]	FF [%]	PCE [%]
Without	Forward	1.07	22.24	58.62	13.92
	Reverse	1.08	22.12	59.33	14.11
	Average	1.07 ± 0.01	22.04 ± 1.32	58.76 ± 2.17	13.94 ± 1.54
With	Forward	1.07	23.95	76.51	19.64
	Reverse	1.08	23.92	80.36	20.82
	Average	1.07 ± 0.01	23.43 ± 0.88	79.16 ± 1.95	20.02 ± 1.38

Table S6. Crystal data and structure refinement for compound 1.

1·H₂O			
Formula	C ₅₁ H ₄₄ BF ₄ IrO ₈ P ₂	μ [mm ⁻¹]	7.085
Mr	1125.79	<i>F</i> (000)	1120.0
Temperature/ K	100.01(10)	Crystal size [mm ³]	0.20 × 0.20 × 0.10
Crystal system	triclinic	Radiation (Å)	CuK α (λ = 1.54184)
Space group	<i>P</i> -1	θ range [°]	4.111 to 78.138
<i>a</i> [Å]	11.21890(10)	Index ranges	-14 ≤ <i>h</i> ≤ 14, -15 ≤ <i>k</i> ≤ 14, -17 ≤ <i>l</i> ≤ 23
<i>b</i> [Å]	11.9271(2)	Reflns collected	26000
<i>c</i> [Å]	18.8998(3)	Independent reflns	9102
α [°]	78.7620(10)	Observed reflns [<i>I</i> ≥ 2 σ]	21075
β [°]	78.8080(10)	Data/restraints/para ms	9102/0/633
γ [°]	65.3690(10)	GOF on <i>F</i> ²	1.091
<i>V</i> [Å ³]	2236.63(6)	<i>R</i> ₁ / <i>wR</i> ₂ [<i>I</i> ≥ 2 σ (<i>I</i>)]	0.0357/0.0911
<i>Z</i>	2	<i>R</i> ₁ / <i>wR</i> ₂ all data)	0.0422/0.0995
ρ_{calcd} [gcm ⁻³]	1.669	Largest peak/hole [e Å ⁻³]	1.84/-1.94

Table S7. Selected bond lengths (Å) and angles (°) for compound 1.

Bond lengths (Å)		Bond angles (°)	
Ir1–C1	2.110(4)	Ir1–C1–C2	107.3(3)
Ir1–C4	2.080(4)	Ir1–C4–C3	115.7(3)
Ir1–O2	2.164(3)	Ir1–C4–C5	122.7(3)
Ir1–C8	1.931(5)	Ir1–O2–C7	125.9(3)

C1–C2	1.524(6)	Ir1–C8–O3	172.9(4)
C2–C3	1.468(6)	C1–Ir1–C4	80.48(17)
C3–C4	1.352(6)	C4–Ir1–O2	90.02(14)
C4–C5	1.448(6)	C1–C2–C3	113.6(4)
C5–C6	1.359(6)	C2–C3–C4	115.9(4)
C6–C7	1.435(7)	C4–C5–C6	126.4(4)
C5–C9	1.508(6)	C5–C6–C7	127.3(4)
C6–C11	1.517(6)	C1–C2–O1	121.7(4)
C9–C10	1.553(6)	C3–C2–O1	124.7(4)
C10–C11	1.544(7)	C202–C1–Ir1	114.9(3)
C2–O1	1.224(5)	C1–Ir1–P2	84.26(12)
C7–O2	1.244(6)	C2–C1–C202	105.0(3)
C8–O3	1.130(6)		

9. References

- [S1]O. V. Dolomanov, L. J. Bourhis, R. J. Gildea, J. A. K. Howard, H. Puschmann, Puschmann, OLEX2: a Complete Structure Solution, Refinement and Analysis Program. *J. Appl. Cryst.* **2009**, *42*, 339-341.
- [S2]G. M. Sheldrick, SHELXT-Integrated Space-group and Crystal-structure Determination. *Acta Cryst., Sect. A.* **2015**, *71*, 3-8.
- [S3]G. M. Sheldrick, Crystal Structure Refinement with SHELXL. *Acta Cryst., Sect. C.* **2015**, *71*, 3-8.
- [S4]a) Y. Zhao, D. G. Truhlar, A New Local Density Functional for Main-group Thermochemistry, Transition Metal Bonding, Thermochemical Kinetics, and Noncovalent Interactions. *J. Chem. Phys.* **2006**, *125*, 194101-194118; b) D. Andrae, U. Häussermann, M. Dolg,

H. Stoll, H. Preuß, Energy-adjusted ab Initio Pseudopotentials for the Second and Third Row Transition Elements. *Theo. Chim. Acta.* **1990**, *77*, 123-141.

[S5]a) A. D. Becke, Density-functional Thermochemistry. III. The Role of Exact Exchange. *J. Chem. Phys.* **1993**, *98*, 5648-5652; b) J. P. Perdew, K. Burke, Y. Wang, Generalized Gradient Approximation for the Exchange-correlation Hole of a Many-electron System. *Phys. Rev. B* **1996**, *54*, 16533-16539.

[S6]M. Frisch, G. Trucks, H. B. Schlegel, G. E. Scuseria, M. A. Robb, J. R. Cheeseman, G. Scalmani, V. Barone, B. Mennucci, G. Petersson, *gaussian 09, Revision d. 01, Gaussian*, **2009**, Vol. 201.

[S7]a) G. Kresse, J. Furthmüller, Efficiency of Ab-initio Total Energy Calculations for Metals and Semiconductors Using a Plane-wave Basis Set. *Comp. Mater. Sci.* **1996**, *6*, 15-50; b) J. P. Perdew, K. Burke, M. Ernzerhof, Generalized Gradient Approximation Made Simple. *Phys. Rev. Lett.* **1996**, *77*, 3865-3868.